

Drift velocity peak and negative differential mobility in high field transport in graphene nanoribbons

A. Betti,* G. Fiori, and G. Iannaccone

*Dipartimento di Ingegneria dell'Informazione: Elettronica,
Informatica, Telecomunicazioni, Università di Pisa,
Via Caruso 16, I-56122, Pisa, Italy*

Abstract

Drift velocity in suspended armchair graphene nanoribbons (A-GNRs) does not saturate with increasing electric field, but exhibits a maximum. The velocity peak and the following negative differential mobility are due to the quasi-linear dispersion relation of GNRs for relatively small wave vectors and to the onset of optical phonon emission. This mechanisms explains also the similar effect observed in zigzag CNTs. Single-particle full-band Monte Carlo simulations show that drift velocity can reach 4×10^5 m/s in 10 nm-wide GNRs for an electric field ≈ 10 kV/cm, corresponding to average electron energy larger than 10 times the thermal energy. Velocity peak does not depend on charge density for concentration up to 10^{12} cm $^{-2}$. GNRs deposited on HfO $_2$ exhibit a drift velocity degraded by up to a factor of ≈ 10 with respect to suspended GNRs and increasing linearly up to fields above 10 kV/cm.

* E-mail: alessandro.betti@iet.unipi.it

Assessing the potential of Graphene Nanoribbons (GNRs) for future electronic applications requires full understanding of both quasi-equilibrium and far-from-equilibrium transport mechanisms [1, 2]. In contrast to the outstanding mobility measured in 2D graphene sheets (close to 10^5 cm²/Vs near room temperature [3]), experimental low-field mobility in GNRs can be almost three orders of magnitude smaller and is limited by edge disorder [1, 4]. Furthermore, we know that achieving ideally smooth edges is not enough: full-band modeling shows that low-field mobility due to only acoustic (AC) phonon scattering at low fields is close to 500 cm²/Vs for 1 nm-wide GNRs [5, 6].

Most importantly, nanoscale transistors do not operate in the low-field mobility limit. Therefore, simulation of far of equilibrium transport conditions is required to understand achievable device performance. Whereas at low field carrier scattering is mainly due to low-energy intravalley acoustic phonons [5, 6], at high electric field scattering is dominated by optical phonon emission (EM), which becomes relevant when electrons gain enough energy to emit optical phonons.

High-field steady-state transport can be simulated by solving the Boltzmann transport equation (BTE) through the single-particle Monte Carlo (MC) method.

When dealing with 1D systems, however, particular attention has to be paid in accurately describing the energy dispersion relation due to quantum lateral confinement: for each GNR subband there is a parabolic behavior close the subband minimum, and then the typical graphene quasi-linear behavior already for relatively small wavevector values, corresponding to a velocity $\approx 8 \times 10^5$ m/s. Some authors have considered phonon confinement and multisubband transport, focusing on quantum wires with the effective mass approximation [7, 8]. For GNRs, a multisubband MC approach has been followed in [9] and BTE has been solved in a deterministic way at criogenic temperatures in [10]. Bresciani *et al.* [11] have used a 2D model, which is not fully adequate for sub-10 nm GNRs, where size effects are indeed relevant [6].

In this work, we adopt a steady-state single-particle full band MC approach accounting for carrier degeneracy [12, 13], which has a significant effect at typical concentrations for materials with a small density of states as graphene. Scattering rates are obtained within the Deformation Potential Approximation (DPA) from phonon dispersions described by means of the fourth-nearest-neighbour force-constant approach (4NNFC) [14] and a p_z tight-binding Hamiltonian for the electronic structure. In particular, we take into account in-plane

longitudinal acoustic and optical (LA and LO), transversal optical (TO) and surface optical (SO) phonons. In each subband, the rates are computed on a 2000-point grid in the k_x -space (due to symmetry only longitudinal electron wavevector $k_x > 0$ have been taken into account), considering energy up to 1.5 eV above the bottom of the first subband and including up to 18 subbands: this ensures accurate results even for strong longitudinal electric field $F \leq 10^2$ kV/m and for all the considered GNR widths ($W \leq 10$ nm). Due to Van Hove singularities in the 1D rates, the self-scattering method [15] results to be inefficient, so that we have adopted the Monte Carlo procedure described in Ref. [15], extended to quasi-1D systems and explained in details in Ref. [16].

The whole story of an electron has a duration $T = \sum_i \Delta t_i$ (we have considered up to 10-100 μs depending on W and F), where $\Delta t_i = t_{i+1} - t_i$ is the i -th time step and t_i is the i -th sampled time. At each t_i , the wavevector $\mathbf{k} = (k_x, k_{y\eta})$, where $k_{y\eta}$ is the transverse quantized electron wavevector [5, 6], is computed and the average value of quantity X (either the drift velocity $v(\mathbf{k}) = 1/\hbar \cdot \partial E(\mathbf{k})/\partial k_x$ or the energy $E(\mathbf{k})$) is evaluated according to [15]:

$$\langle X \rangle_t = \frac{1}{T} \int_0^T X[k_x(t')] dt' = \frac{1}{T} \sum_{t_i} \int_{t_i}^{t_{i+1}} X[k_x(t')] dt'. \quad (1)$$

The electronic temperature T_{el} under an applied homogeneous field F is also computed by equating $\langle v(k_x)^2 \rangle$ with the analytical formula of the mean square velocity at equilibrium

$$\langle v^2 \rangle_0 = \frac{\sum_{k_{y\eta}} \int dE v^2(\mathbf{k}) D_\eta(\mathbf{k}) f[E(\mathbf{k}) - E_F]}{\sum_{k_{y\eta}} \int dE D_\eta(\mathbf{k}) f[E(\mathbf{k}) - E_F]}, \quad (2)$$

where $D_\eta(\mathbf{k}) = 1/\pi [dk_x/dE(\mathbf{k})]$ is the 1D density of states (DOS) for the η -th electron subband and $f(E)$ is the Fermi occupation factor. For $F = 0$, T_{el} is equal to the lattice room temperature T_{lat} , whereas for $F > 0$, $T_{el} > T_{lat}$. Once obtained T_{el} , the distribution function is updated accordingly at each t_i and final states for scattering are filled obeying to the Pauli exclusion principle.

The computed average drift velocity $\langle v_d \rangle$ limited by intrinsic phonons is plotted in Fig. 1a as a function of F for suspended sub-10 nm GNRs and for a carrier density $n_{2D} = 10^{12} \text{ cm}^{-2}$. $\langle v_d \rangle$ strongly varies within the considered F interval and a maximum appears at high electric field ($F = F_{th}$). For $F < F_{th}$, $\langle v_d \rangle$ can be fitted by means of the Caughey-Thomas model, i.e. $\langle v_d(F) \rangle = (\mu_{in,0} F) / [1 + (\mu_{in,0} F / v_p)^\gamma]^{1/\gamma}$, where $\gamma \approx (1.3 \div 2)$, $\mu_{in,0}$ is the intrinsic low-field mobility and v_p is the peak velocity, which ranges from 2×10^5 to 4×10^5 m/s, depending on W (Table I).

Velocity does not saturate with F , analogously to what has been observed in the case of zigzag CNTs [17, 18]. As shown in Fig. 1a, $\langle v_d \rangle$ slightly decreases for increasing F [17]. However, in contrast to what is claimed in [17], the negative differential mobility cannot be explained by the increased number of populated states in the second subband with smaller $v(\mathbf{k})$. Indeed, as in [18], we have verified for $W = 10$ nm that such effect is much more pronounced if we fictitiously limit transport to only one subband (red dashed line in Fig. 1a).

The velocity peak can be explained by the combined effect of the quasi-linear dispersion relation in GNRs and the strong increase of optical emission at high F , which increases the occurrence of backscattering events therefore reducing the average velocity. If we follow the story of a single electron, we can see that as F increases, instantaneous electron velocity cannot increase beyond the limit imposed by the dispersion relation: Any backscattering event will invert the instantaneous velocity sign and therefore reduce the average velocity. Therefore, in the absence of optical phonon emission, the drift velocity $\langle v_d \rangle$ would saturate to about 8×10^5 m/s. The onset of optical phonon emission makes $\langle v_d \rangle$ peak at a fraction of that value and then decrease with F . We believe that the very same mechanism explains also the negative differential mobility in zigzag CNTs, even if it has not been proposed before [17, 18].

One can also see that the peak velocity v_p increases with W . Indeed, if $\hbar\omega$ is the optical phonon energy (≈ 160 meV for LA modes [6]), the current J can be estimated as $J = \frac{4e}{h} \hbar\omega \frac{E_F}{\pi \hbar v_F}$ [19], where v_F is the Fermi velocity. Since $v_p = J/(en_{2D})$ and the Fermi wavevector $k_F = \pi n_{2D} W$, we obtain $v_p = \omega \times W/\pi \propto W$.

The threshold field F_{th} strongly decreases with W , because of the increased mean free path $\langle L_{\mathbf{k}} \rangle$, which allows electrons to gain energy required to emit optical phonons at lower F . F_{th} can be roughly estimated by imposing the cutoff energy $\hbar\omega$ for optical emission equal to the mean kinetic energy gained between two scattering events, i.e. $qF_{th}\langle L_{\mathbf{k}} \rangle$. Since by increasing W from 1 to 10 nm, $\langle L_{\mathbf{k}} \rangle$ increases from ≈ 6 nm to 1 μm [5, 6], F_{th} decreases from $\approx 2.7 \times 10^2$ kV/cm to ≈ 1.6 kV/cm. We remark also that the obtained values for $\langle v_{in} \rangle$ are in agreement with those found for zigzag CNTs with a circumference comparable with the considered W , both in linear and in non-linear regimes [17]. In Fig. 1b, $\langle v_d \rangle$ is plotted as a function of n_{2D} for $F = 10$ kV/cm: $\langle v_d \rangle$ does not depend on n_{2D} even in the degenerate regime ($n_{2D} = 10^{12} \text{ cm}^{-2}$), where the Pauli principle limits up to the 50% of the scattering

events.

In Fig. 2, we show the intrinsic mobility $\mu_{in} \equiv \langle v_d \rangle / F$ as a function of F for $n_{2D} = 10^{12} \text{ cm}^{-2}$. Since in the linear transport regime $v_d \propto F$, μ_{in} is constant for $F \leq F_{th}$ and decreases above F_{th} as $\mu_{in} \propto 1/F^\alpha$ with $\alpha > 1$. In addition, the narrower the ribbons, the stronger the suppression due to lateral confinement. Results are in good agreement with a multi-subband model for 5 nm-wide GNRs [9]. In the inset of Fig. 2, the average electron energy $\langle E_{\mathbf{k}} \rangle$ in units of kT_{lat} as a function of F for W ranging from 1 to 10 nm is shown for $n_{2D} = 10^{12} \text{ cm}^{-2}$. While for low $F \approx 0.1 \text{ kV/cm}$ electrons tend to remain near the first conduction subband edge with $\langle E_{\mathbf{k}} \rangle \approx kT_{lat}$, for high field $F \geq 10^2 \text{ kV/m}$ $\langle E_{\mathbf{k}} \rangle \gg kT_{lat}$ and higher energy states are occupied. In particular, a negative slope $d\langle E_{\mathbf{k}} \rangle / dF$ appears for $F > F_{th}$, due to optical emission which limits the maximum energy achievable by electrons and can be considered the cause of the decrease of $\langle v_d \rangle$ at high F . Close to F_{th} , $\langle E_{\mathbf{k}} \rangle$ increases with increasing W , since conduction subbands become closer, allowing electrons to populate higher subbands.

In Fig. 3a the distribution function G is shown as a function of the energy for $F = 1$ and 10^2 kV/cm ($W = 4.86 \text{ nm}$). At low fields, $G(E)$ decreases rapidly with energy, showing sharp peaks due to intersubband scattering. At high fields, electrons are pushed up to energies well above 1 eV, enhancing T_{el} (inset of Fig. 2) and optical phonon emission. This is clearly confirmed by Fig. 3b, where the relative ratio of scattering events for the different mechanisms are shown as a function of F . For $F \leq 1 \text{ kV/cm}$, the main scattering events involve absorption (ABS) and emission of LA phonons. For $F \geq 10^2 \text{ kV/cm}$, optical phonon emission (of both LO and TO phonons) becomes predominant, increasing up to 30% of the total number of events. In Fig. 3c the relative time spent by an electron in a subband, i.e. the relative subband occupancy, is shown as a function of F for $W = 4.86 \text{ nm}$. As can be seen, close to $F_{th} \approx 10 \text{ kV/cm}$ the higher subbands become more populated with increasing F and an inversion of population occurs.

In Fig. 4a the average drift velocity $\langle v_d \rangle$ is shown as a function of F for GNRs deposited on SiO_2 [5, 6] including the effect of SO phonons, through the first SO(1) and second SO(2) modes ($n_{2D} = 10^{11} \text{ cm}^{-2}$). $\langle v_d \rangle$ for suspended ribbon is 2 to 3 times larger than that for GNR on SiO_2 . The electric field activating SO phonon emission is almost equal to $(\hbar\omega_{SO})/(q \times \langle L_{\mathbf{k}} \rangle)$ ($\hbar\omega_{SO} = 58.9 \text{ meV}$ for SO(1) mode). Since the mean free path $\langle L_{\mathbf{k}} \rangle$ due to remote phonons is comparable to that accounting for only intrinsic phonons [5, 6], the activating field is at least 3 times smaller than that in suspended GNR. As a consequence,

scattering involving SO(1) phonons happens very often already for $F = 1$ kV/cm, as can be seen in Fig. 4b for $W = 2.62$ nm. Note however that the linear region tends to extend to higher F with respect to the intrinsic case, due to the large absorption rate of SO(1) phonons (Fig. 4b) associated to the high Bose-Einstein occupation factor [6], which counterbalances SO(1) emission. For GNR deposited on HfO₂, $\langle v_d \rangle$ is suppressed by up to a factor 10 with respect to suspended GNRs and, for narrow ribbons, does not saturate even for fields up to 10^2 kV/cm.

In conclusion, we have performed a full-band investigation of the dependence of drift velocity and mobility on the electric fields in GNRs. Suspended GNRs exhibit a drift velocity peak and then a negative differential mobility for large electric field, as has been also observed in zigzag CNTs. We demonstrated that this property is due to the combined effect of graphene linear dispersion relation and the emission of optical phonons. In particular, the maxima occur for a threshold field F_{th} roughly proportional to $1/\langle L_{\mathbf{k}} \rangle \propto 1/W$. The same mechanism also explains negative differential mobility in zigzag CNTs. GNR deposition on SiO₂ (HfO₂) substrate strongly degrades $\langle v_d \rangle$ by a factor 2-3 (≈ 10), and correspondingly pushes velocity saturation and peak to higher electric fields.

Authors gratefully acknowledge support from the EU FP7 Project NANOSIL (n. 216171), GRAND (n. 215752) grants, and by the MIUR-PRIN project GRANFET (Prot. 2008S2CLJ9) via the IUNET consortium.

-
- [1] X. Wang, Y. Ouyang, X. Li, H. Wang, J. Guo, and H. Dai, Phys. Rev. Lett. **100**, 206803 (2008).
 - [2] A. Betti, G. Fiori, and G. Iannaccone, IEEE Trans. Electron Devices (DOI:10.1109/TED.2010.2100045, 2011).
 - [3] K. I. Bolotin, K. J. Sikes, J. Hone, H. L. Stormer, and P. Kim, Phys. Rev. Lett. **101**, 096802 (2008).
 - [4] Y. Yang and R. Murali, IEEE Elec. Dev. Lett. **31**, 237 (2010).
 - [5] A. Betti, G. Fiori, and G. Iannaccone, Appl. Phys. Lett. **98**, 212111 (2011).
 - [6] A. Betti, G. Fiori, and G. Iannaccone, unpublished (2011).
 - [7] S. Briggs and J. P. Leburton, Phys. Rev. B **38**, 8163 (1988).

- [8] R. Mickevicius, V. V. Mitin, K. W. Kim, and M. A. Stroscio, *Semicond. Sci. Technol.* **7**, B299 (1992).
- [9] L. Zeng, X. Y. Liu, G. Du, J. F. Kang, and R. Q. Han, *Int. Conf. Simulation of Semiconductor Processes and Devices* pp. 1–4 (2009).
- [10] D. Huang, G. Gumbs, and O. Roslyak, *Phys. Rev. B* **83**, 115405 (2011).
- [11] M. Bresciani, P. Palestri, and D. Esseni, *Solid-State Electronics* **54**, 1015 (2010).
- [12] M. Zebarjadi, C. Bulutay, K. Esfarjani, and A. Shakouri, *Appl. Phys. Lett.* **90**, 09211 (2007).
- [13] P. Lugli and D. K. Ferry, *IEEE Trans. Electron Devices* **32**, 2431 (1985).
- [14] R. Saito, G. Dresselhaus, and M. Dresselhaus, Imperial College Press, London (2003).
- [15] C. Jacoboni and L. Reggiani, *Rev. Mod. Phys.* **55**, 645 (1983).
- [16] See EPAPS supplementary material at [\[1\]](#) for the Monte Carlo procedure.
- [17] G. Pennington and N. Goldsman, *Phys. Rev. B* **68**, 045426 (2003).
- [18] V. Perebeinos, J. Tersoff, and P. Avouris, *Phys. Rev. Lett.* **94**, 086802 (2005).
- [19] M. Freitag, M. Steiner, Y. Martin, V. Perebeinos, Z. Chen, J. C. Tsang, and P. Avouris, *Nano Lett.* **9**, 1883 (2009).

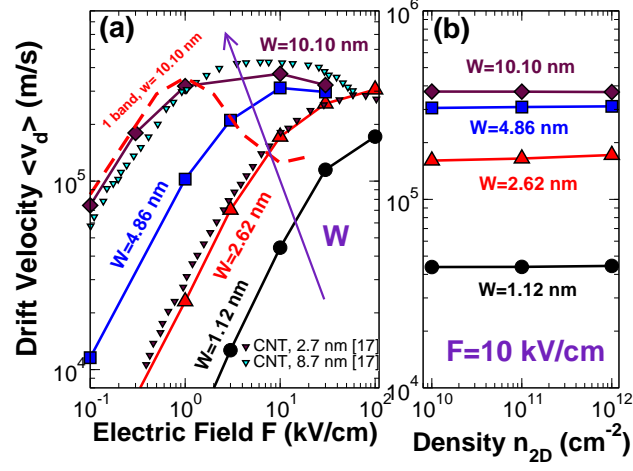


FIG. 1. (Color online) (a) Average drift velocity $\langle v_d \rangle$ as a function of F ($n_{2D} = 10^{12}$ cm $^{-2}$) and (b) as a function of n_{2D} for different W of suspended GNRs. In (a) results from MC simulations for zigzag CNTs [17] with sub-10 nm circumference (2.7 nm and 8.7 nm) are also reported. In (b) $F = 10$ kV/cm.

TABLE I. Caughey-Thomas parameters $\mu_{in,0}$, v_p and γ for different W , obtained through the fitting with MC data.

| W (nm) | $\mu_{in,0}$ (cm ² /Vs) | v_p (m/s) | γ |
|----------|------------------------------------|-------------------|----------|
| 1.12 | 310 | 2.2×10^5 | 1.7 |
| 2.62 | 2700 | 3.2×10^5 | 1.3 |
| 4.86 | 12000 | 3.3×10^5 | 1.4 |
| 10.10 | 80000 | 3.7×10^5 | 2 |

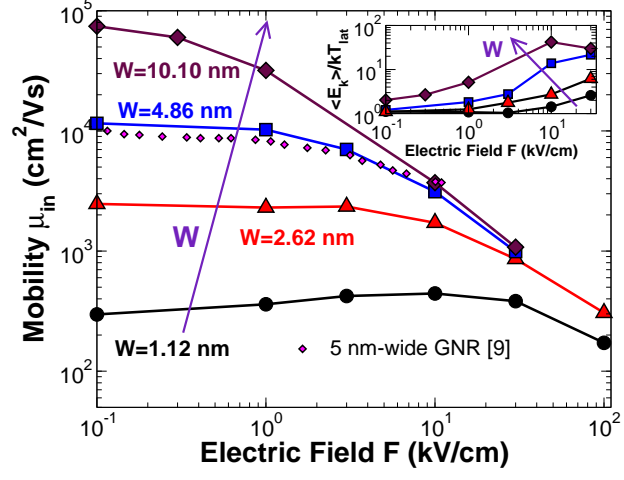


FIG. 2. (Color online) (a) Intrinsic mobility μ_{in} and (Inset) average electron energy as a function of F for different W . Results for GNRs with $W = 5$ nm [9] are also shown in (a). $n_{2D} = 10^{12}$ cm⁻².

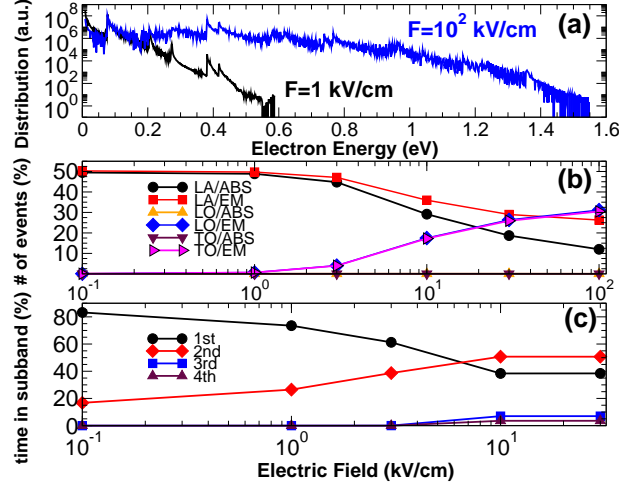


FIG. 3. (Color online) (a) Energy distribution function for $F = 1$ and 10 kV/cm. (b) Fraction of different scattering events as a function of F . (c) Fraction of time spent by an electron in a subband as a function of F . $W = 4.86$ nm.

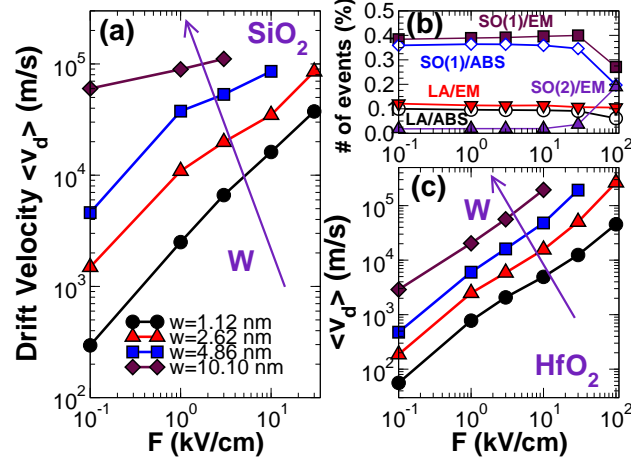


FIG. 4. (Color online) (a) Average drift velocity $\langle v_d \rangle$ and (b) fraction of the predominant scattering events as a function of F for GNR on SiO_2 . (c) $\langle v_d \rangle$ as a function of F for GNR on HfO_2 . In (b) $W = 2.62$ nm. $n_{2D} = 10^{11} \text{ cm}^{-2}$.